# Important considerations in optimising the structural aspect of a SDOF electromagnetic vibration energy harvester

Faruq Muhammad Foong, Chung KetThein, Daniil Yurchenko

University of Nottingham
UK | CHINA | MALAYSIA

University of Nottingham Ningbo China, 199 Taikang East Road, Ningbo, 315100, Zhejiang, China.

First published 2020

This work is made available under the terms of the Creative Commons Attribution 4.0 International License:
http://creativecommons.org/licenses/by/4.0

The work is licenced to the University of Nottingham Ningbo China under the Global University Publication Licence:
https://www.nottingham.edu.cn/en/library/documents/research-support/global-university-publications-licence-2.0.pdf

University of Nottingham
UK | CHINA | MALAYSIA

# Important considerations in optimising the structural aspect of a SDOF electromagnetic vibration energy harvester

Faruq Muhammad Foong[1], Chung Ket Thein*[,2], Daniil Yurchenko[3]

[1]School of Engineering and Physical Sciences, Heriot-Watt University, No. 1, Jalan Venna P5/2, Precinct 5, 62200 Malaysia
[2]School of Aerospace, University of Nottingham Ningbo China, Ningbo 315100, PR China
[3]School of Engineering and Physical Sciences, Heriot-Watt University, Edinburgh EH14 4AS, United Kingdom
*Corresponding author. E-mail address: chungket.thein@nottingham.edu.cn.

**Abstract**

This study investigates several important considerations to be made when optimising the structural aspects of a single-degree-of-freedom (SDOF) electromagnetic vibration energy harvester. Using the critically damped stress method, the damping and power output of the harvester were modelled and verified, displaying an excellent agreement with the experimental results. The SDOF harvester was structurally optimised under a certain set of constraints and it was found that under the fixed beam's thickness condition, the harvester displayed an insignificant increase in power output as a function of volume when the device's size was relatively larger. This highlights the importance of considering a smaller practical volume for this case. Additionally, when optimising the device using a low stress constraint and a low damping material, it was observed that considering the load resistance as an input parameter to the objective function would lead to a higher power output compared to the optimum load resistance condition. Further analysis indicated that there exists a power limit when the electromagnetic coupling coefficient approaches infinity. For the case of a high electromagnetic coupling coefficient value and a small volume constraint, it is possible to achieve approximately 80.0% of the harvester's power limit. Finally, it was demonstrated that a high power output can be achieved for a SDOF electromagnetic harvester by considering a high-density proof mass centred at the free end of the beam.

*Keywords: Electromagnetic energy harvesting; Damping; Structural optimisation; SDOF; Power*

## 1. Introduction

Energy harvesting from ambient vibrations have continued receiving the interest of many researchers over the past two decades. The idea of providing a green and sustainable source of energy to power low-consumption electronics is attractive as it allows small devices such as a wireless sensor node to operate in remote areas where the use of conventional batteries may be inconvenient. Additionally, it is also cheaper to use such a device for long term applications [1–3]. However, over the past decade, energy harvesting has also been extended for large-scale applications [4–6]. Among the available ambient sources for energy harvesting, mechanical vibrations have emerged as one of the most promising option. While vibration energy harvesting provides an excellent alternative to replace batteries, there are still two main concerns in this field. The first concern is that the output power of a vibration energy harvester is strongly reliant on its vibration input source. However, ambient vibrations are generally low in frequency and magnitude, which may limit the performance of the harvester. Secondly, a vibration energy harvester has a limited frequency bandwidth. Generally, the harvester would only produce useful power output when its resonant frequency matches the frequency of the ambient vibration source. If the frequency of the vibration source deviates slightly, the power output would drop significantly. In some practical applications, the frequency of the vibration source is not constant and can fluctuate. Thus, the research in the optimisation of vibration energy harvesters has become vastly popular, with the aim to produce a high-efficiency output harvester.

Despite being a main issue, it is actually difficult to optimise the frequency bandwidth of a harvester as the definition of an 'optimum' frequency bandwidth is vague and maximising the bandwidth would generally take a large toll on the power output. Hence, most studies would focus on methods to improve the frequency bandwidth instead of optimising it [7–9]. In contrast, many studies have been conducted to optimise the power output of a vibration energy harvester. The most common

example of power output optimisation in vibration energy harvesting applications is the determination of the optimum load resistance that corresponds to the maximum power output of the harvester, which have been reported in many published works [10–13], among others. Generally, optimisation of a vibration energy harvester can be divided into two streams. The first stream is the structural side, which represents the non-electrical components of the harvester. Optimisation in this aspect usually involves physical changes to the structure such as its shape or its dimensions. The second optimisation stream depends on the electrical conversion method of the harvester and is focused on optimisation of the electrical parameters of the harvester. For electromagnetic harvesters, the optimisation can either focus on the electromagnetic side, the structural components or both.

Typically, optimisation performed on the electromagnetic aspect considers maximising the electromagnetic coupling between the coil and the magnets by either increasing the magnetic flux density [14,15], optimising the coil layout [16] or simultaneously optimising both the coil and the magnet components [17]. Beeby et al. [18] optimised the magnet dimension of a cantilevered electromagnetic harvester using a finite element approach. The optimised magnet dimensions resulted in 2.6 times increase in voltage output as compared to the original magnets. Tang et al. [19] optimised a tubular electromagnetic harvester by considering a double layer configuration using a combination of radial and axial magnets, which increased the power output of their original design by 280%. On the structural side, Kapanen [20] noted that the most important factor to consider when optimising a single-degree-of-freedom (SDOF) electromagnetic harvester under a constrained volume is to maximise the mass of the vibrating object, since the power output of the harvester is proportional to the mass squared. Chiu et al. [21] performed an analytical optimisation of a two-degree-of-freedom electromagnetic harvester by considering eight design parameters, which included both the electromagnetic and the structural parameters. On the other hand, Joubaneh and Barry [22] took a slightly different approach where they attempted to optimise the structural and electromagnetic aspect of an electromagnetic resonant shunt tuned mass damper-inerter, which acts as both an energy harvester and a vibration suppressor. In this case, it was important to consider the trade-off between the two conflicting functions and find a configuration that would maximise both performances. Other authors have also presented methods to improve the structural performance of an electromagnetic harvester [23–26]. However, these studies were dedicated to the enhancements instead of a real structural optimisation. In other words, studies that focuses on a real structural optimisation of electromagnetic harvesters are quite rare.

In this paper, several important considerations were investigated and highlighted regarding the optimisation on the structural aspect of a SDOF electromagnetic vibration energy harvester. The mathematical model for the harvester was first derived using the Euler-Bernoulli beam theory and the critically damped stress method and verified experimentally. A structural optimisation was then performed for the SDOF harvester under several different constraints. The first consideration addressed in this paper is whether a larger practical volume constraint will generally lead to a higher power output when optimised. Secondly, the conditions at which two different load resistance constraints should be considered in the optimisation process to maximise the resulting power output was analysed. After that, the expression for the power limit of a SDOF electromagnetic harvester was derived and the portion of the power limit that was considered to be practically achievable was determined. Finally, the ideal proof mass geometry to maximise the power output the harvester was obtained and based on this ideal output, some practical considerations regarding the geometry and placement of the proof mass were highlighted.

## 2. Governing equations for SDOF cantilever-based electromagnetic vibration energy harvester

Consider a typical SDOF cantilever-based electromagnetic vibration energy harvester design as seen in Fig. 1.

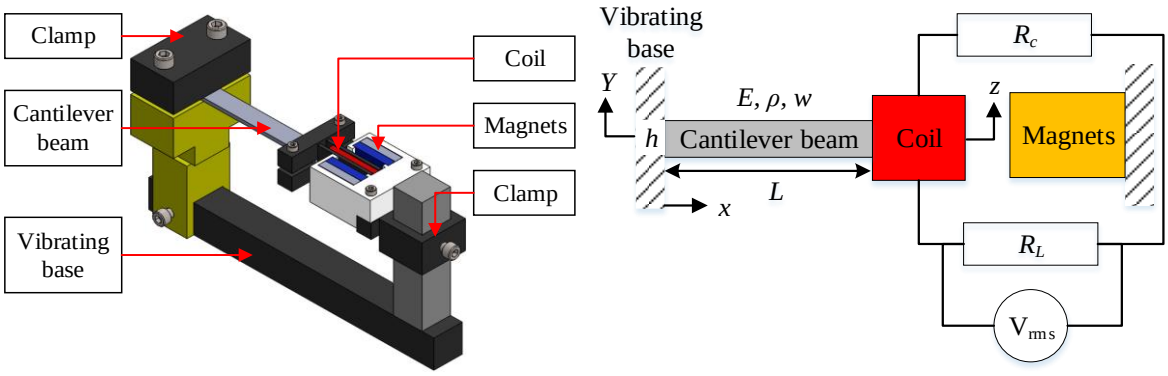


**Fig. 1.** Design (left) and schematic (right) of a cantilevered electromagnetic vibration energy harvester.

The design consists of a rectangular cantilever beam clamped at one end whereas a conducting coil was fixed to its other end. The variables $E$, $\rho$, $L$, $h$, and $w$ defines the cantilever beam's Young's modulus, density, length, thickness and width. The $x$ variable represents the position along the beam's length. The coil has an inertial resistance $R_c$ and is connected in series to a load resistor, $R_L$. The clamped end of the beam and the magnets are fixed onto a base that is vibrating with an acceleration amplitude of $G$.

### 2.1 Voltage and power equations

Based on Faraday's law of electromagnetic induction, the root-mean-squared (RMS) voltage induced in the load resistance, $V_{rms}$, as the coil vibrates through the magnetic field of the magnets is

$$V_{rms} = \frac{K}{\sqrt{2}} v_c \frac{R_L}{R_L + R_c} \tag{1}$$

$$K = NBlf \tag{2}$$

where $N$, $l$ and $f$ is the number of turns, effective length and fill factor of the coil, $B$ is the average magnetic flux density of the magnets and $v_c$ is the vibrating velocity of the coil. According to Ohm's electrical law, the average power output at the load resistance, $P_{ave}$, is

$$P_{ave} = \frac{{V_{rms}}^2}{R_L} \tag{3}$$

It is worth noting that in Eqs. (1) and (2), if the properties of the electromagnetic components are fixed, the power output of the harvester would solely depend on the velocity of the coil.

### 2.2 Equation of motion of the cantilever under a harmonic base excitation

The dynamics of the SDOF harvester in Fig. 1 can be modelled as a cantilever beam with a proof mass attached on its free end. Assuming a constant, harmonic base acceleration input and applying the Euler-Bernoulli beam theory, the absolute amplitude of a vibrating cantilever beam at position $x$ and time $t$ can generally be expressed as [27]

$$z_a(x,t) = z(x,t) + \frac{G}{\omega^2} e^{i\omega t} \tag{4}$$

where $z(x,t)$ is the vertical displacement of the cantilever beam relative to the vibrating base, $G$ is the acceleration of the harmonic base excitation input and $\omega$ is the driving frequency. Applying the Fourier method, $z(x,t)$ can be separated in terms of its spatial and time components.

$$z(x,t) = \sum_{n=1}^{\infty} \varphi_n(x)\eta_n(t) \tag{5}$$

where $\varphi_n$ is the mass normalized eigenfunction of the beam and $\eta_n$ is the response function. The subscript $n$ in Eq. (5) corresponds to the vibration mode of the beam. However, for a SDOF harvester,

only the first mode ($n = 1$) is normally considered as the response at this mode is significantly larger than that of the higher modes. Considering the case of the first mode resonance, the beam eigenfunction and response function can be written as

$$\varphi_1(x) = C_1\left[\cosh\frac{\lambda_1}{L}x - \cos\frac{\lambda_1}{L}x - J_1\left(\sinh\frac{\lambda_1}{L}x - \sin\frac{\lambda_1}{L}x\right)\right] \tag{6}$$

$$\eta_1(t) = \frac{G\mathrm{e}^{\mathrm{i}\omega t}F_1}{{\omega_1}^2-\omega^2+\mathrm{i}2\zeta_1\omega_1\omega} \tag{7}$$

$$F_1(t) = \frac{m_b}{L}\int_0^L \varphi_1(x)\mathrm{d}x + m_t\varphi_1(L) + M_S\frac{\mathrm{d}\varphi_1}{\mathrm{d}x}(L) \tag{8}$$

where $\zeta_1$ is the first mode damping of the beam, $\omega_1$ is the first mode natural frequency of the beam, $F_1$ is the forcing function, $m_b$ and $m_t$ are the mass of the beam and the proof mass, $M_S$ is the static moment at $x = L$ and $C_1$, $\lambda_1$ and $J_1$ are constant terms derived from the boundary conditions and inertial terms of the cantilever beam and coil [28]. Substituting Eqs. (6), (7) and (8) into equation (5) and differentiating it with respect of time $t$ results in an expression describing the transverse velocity of the beam under first mode vibration.

$$v(x,t) = \frac{\omega}{{\omega_1}^2-\omega^2+\mathrm{i}2\zeta_1\omega_1\omega}G\mathrm{e}^{\mathrm{i}\omega t}F_1\varphi_1(x) \tag{9}$$

Eq. (9) is only valid for $0 \le x \le L$, however, the velocity of the attached coil is usually measured at the centre of the coil, which is located at $x > L$. In this case, the velocity of the coil can be estimated as

$$v_c(t) = \frac{\omega}{{\omega_1}^2-\omega^2+\mathrm{i}2\zeta_1\omega_1\omega}G\mathrm{e}^{\mathrm{i}\omega t}F_1[\varphi_1(L) + x_c{\varphi_1}'(L)] \tag{10}$$

where $x_c$ is the distance from the centre of the coil to $x = L$ and ${\varphi_1}'(L)$ is the derivative of the beam's eigenfunction with respect to $x$ at $x = L$. It is important to mention that the damping ratio of the harvester, $\zeta_1$ equals to the sum of the mechanical damping of the beam and the electromagnetic damping from the coil and magnets.

$$\zeta_1 = \zeta_c + \zeta_e \tag{11}$$

While the electromagnetic damping ratio, $\zeta_e$, for the first mode vibration can be approximated by Eq. (12), there is no analytical function established to describe the mechanical damping ratio, $\zeta_c$, of cantilever beams. Note that $d_e$ and $m_e$ in Eq. (12) refers to the electromagnetic damping constant and the effective mass of the beam respectively.

$$\zeta_e = \frac{d_e}{2m_e\omega_1} = \frac{K^2}{2m_e\omega_1(R_L+R_c)} \tag{12}$$

## 3. Evaluation of mechanical damping ratio and fatigue limit stress approximation

For macro-size cantilever beams (volume > 100 mm$^3$), the mechanical damping ratio can be divided into its thermoelastic damping, $\zeta_h$, and its material damping $\zeta_m$ as shown in Eq. (13). Other forms of damping can be assumed negligible for this size range [29].

$$\zeta_c = \zeta_h + \zeta_m \tag{13}$$

Zener [30] and Lifshitz and Roukes [31] proposed different equations to define the thermoelastic damping ratio of the cantilever beams. Nevertheless, the results from both equations are very similar. In this study, Zener's equation was used since it is not bounded by the hyperbolic functions, making it easier to compute for larger frequency values. Equations (14) and (15) describes Zener's thermoelastic damping ratio equation

$$\zeta_h = \frac{E\alpha^2T_0}{2\rho C_p}\frac{\omega\tau}{1+(\omega\tau)^2} \tag{14}$$

$$\tau = \frac{h^2 \rho C_p}{\pi^2 k} \tag{15}$$

where $\alpha$, $C_p$ and $k$ corresponds to the thermal expansion coefficient, specific heat capacity and thermal conductivity of the beam material and $T_0$ is the ambient temperature. In this study, the material damping ratio for the cantilever beam was evaluated using the critically damped stress method proposed by Foong et al. [29]. The method defines a strong relation between the $\zeta_m$ and $\sigma_c$, where $\sigma_c$ is defined as twice the maximum dynamic stress of the beam when vibrated under critically damped condition ($\zeta_1 = 1$). Based on the Euler-Bernoulli beam theory, $\sigma_c$ can be expressed as

$$\sigma_c = EhY \left(\frac{\lambda_1}{L}\right)^2 C_1 F_1 \tag{16}$$

Fig. 2 describes the damping stress relation between the $\zeta_m$ and $\sigma_c$ for four different materials obtained by duplicating the experimental procedures outlined in Foong et al [29].

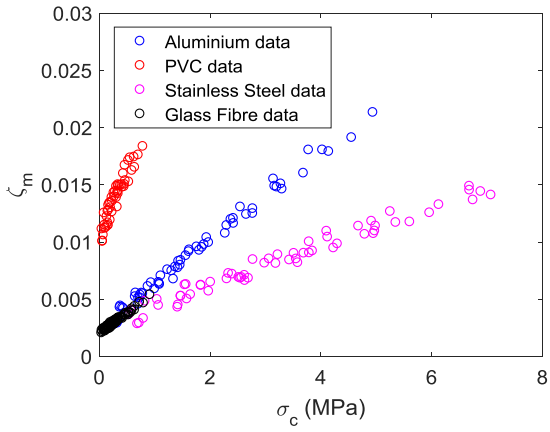


**Fig. 2.** Damping stress relation for aluminium, stainless steel, glass fibre and PVC materials.

All cantilever beams used in the experiment were chosen to meet the criteria of a Euler-Bernoulli beam for first mode vibrations, as described by Labuschagne et al. [32] and Zamiralova and Lodewijks [33], represented in Eqs. (17) and (18).

$$\frac{L}{h} \geq 10 \tag{17}$$

$$\frac{w^2 M}{EIh} \leq 1 \tag{18}$$

where $M$ is the maximum bending moment of the vibrating beam. A best fit curve was fitted to the experimental data of each material. The equations for the best fit curves can be described in the form of

$$\zeta_m = a{\sigma_c}^b + c \tag{19}$$

where the constants of $a$, $b$ and $c$ are tabulated in Table 1.

**Table 1:** Damping stress parameters for four different materials.

| Material | $a$ ($\text{Pa}^{-b}$) | $b$ | $c$ ($\times 10^{-3}$) |
|---|---|---|---|
| Aluminium 1050A | $1.527 \times 10^{-8}$ | 0.9114 | 1.828 |
| PVC | $7.116 \times 10^{-6}$ | 0.5345 | 8.068 |
| Stainless Steel 304 | $2.109 \times 10^{-8}$ | 0.8447 | 1.662 |
| Glass Fibre 10G/40 | $3.567 \times 10^{-9}$ | 1.0000 | 2.001 |

Using Eq. (19) and the constants tabulated in Table 1, it is possible to estimate the material damping ratio of the four different cantilever beams under different conditions. In addition, Thein et al. has shown that the material damping evaluation method here is also applicable for different cantilever-like structures [34]. Based on the dispersion of the experimental data in Fig. 2, one can expect an error margin of up to 10.0% in damping predictions, especially at lower damping values.

Normally, the maximum dynamic stress of the harvester under an operational condition should not exceed its fatigue stress limit, $\sigma_f$, to assure a long lifespan. Lazan [35] reported that for most materials, the relation between a structure's damping energy, $D$, and its maximum vibrating stress, $\sigma_{max}$, can be defined by a two segment curve fit, with one curve defining the relation for when $\sigma_{max} \leq 0.8\sigma_f$ and the other curve for when $\sigma_{max} \geq 0.8\sigma_f$. Both curves can be generalised in the form of

$$D = J{\sigma_{max}}^m \tag{20}$$

where $J$ and $m$ are constants. Assuming a narrow elliptical hysteretic damping model, $\sigma_{max}$ and $D$ can be approximated by

$$\sigma_{max} = \frac{\sigma_c}{2\zeta_m} \tag{21}$$

$$D = \frac{\pi}{E}\sigma_c\sigma_{max} \tag{22}$$

Considering a two-segment curve fit for the relation between $D$ and $\sigma_{max}$, $\sigma_f$ was estimated by determining the intersection point between the two fitted curves as shown in Fig. 3 for aluminium.

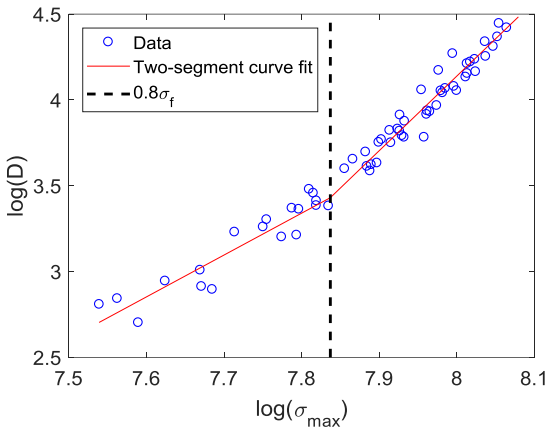


**Fig. 3.** Estimation of fatigue limit stress for aluminium cantilever beam.

The same method was applied for stainless steel and glass fibre. For PVC however, the fatigue limit stress was approximated from literature [36] as a two-segment curve fit was not compatible with the experimental data. The data for PVC was determined to adopt a single-segment curve fit instead. The result of the estimated $\sigma_f$ value for each material is tabulated in Table 2.

## 4. Optimum load resistance

Many past publications have reported the existence of an optimum load resistance value for vibration energy harvesters that results in the harvester's maximum power output. This optimum resistance value can be derived by expanding Eq. (3). Substituting Eqs. (1), (2) and (10) into (3) and considering that maximum power occurs at resonance ($\omega = \omega_1$) results in

$$P_{ave} = \frac{1}{R_L}\left\{\frac{K}{\sqrt{2}}\frac{1}{2(\zeta_c+\zeta_e)\omega_1}GF_1[\varphi_1(L) + x_c{\varphi_1}'(L)]\frac{R_L}{R_L+R_c}\right\}^2 \tag{23}$$

Defining the mechanical damping ratio in terms of its mechanical damping constants where $d_c = 2m_e\omega_1\zeta_c$ and rearranging Eq. (23) results in

$$P_{ave} = \left\{\frac{1}{\sqrt{2}} m_e G F_1 [\varphi_1(L) + x_c \varphi_1{}'(L)]\right\}^2 \frac{K^2 R_L}{[d_c(R_L+R_c)+K^2]^2} \tag{24}$$

Differentiating Eq. (24) with respect to $R_L$ and equating it to zero defines the exact condition of optimum load resistance, $R_L^{opt}$:

$$R_L^{opt} = \frac{K^2}{d_c} + R_c \tag{25}$$

The two most common conditions of the optimum load resistance reported in literatures are $R_L^{opt} = R_c$ and $R_L^{opt} = \frac{K^2}{d_c} - R_c$. The second condition is more commonly recognised as when $\zeta_e = \zeta_m$. Based on Eq. (25), it can be devised that the first condition can only be achieved when $\frac{K^2}{d_c} \ll R_c$ and the second condition is valid when $\frac{K^2}{d_c} \gg R_c$, which is similar to what has been previously reported [37]. Nevertheless, if Eq. (25) is substituted into Eq. (11), it can be shown that under the $R_L^{opt}$ condition, the electromagnetic damping will always be lower or equal to the mechanical damping.

## 5. Verification of the mathematical model for the SDOF design

An experiment was conducted to verify the validity of the developed analytical equations, especially in terms of the damping evaluation. A simple SDOF harvester was created by attaching a coil component to the free end of the cantilever beam using M4 bolts and nuts. A cuboid shaped proof mass was also bonded to the beam using adhesive and positioned just behind the coil as seen in Fig. 4.

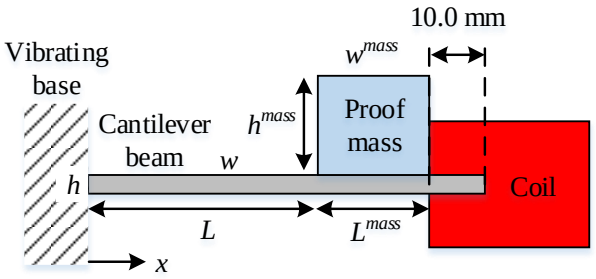


**Fig. 4.** Dimension considerations for a SDOF cantilever-based electromagnetic vibration energy harvester.

where $L^{mass}$, $w^{mass}$ and $h^{mass}$ are the length, thickness and width of the proof mass. The other end of the beam was clamped onto an analogue shaker to induce a harmonic base excitation vibration. Similarly, two pairs of neodymium magnets were also clamped onto the shaker and positioned around the coil. The same magnets and coil components were used throughout the experiment. The air space between the permanent magnets have a $B$ value of 0.26 T and the properties of the coil are $N$ = 250, $l$ = 44.0 mm, $f$ = 0.65 and $R_c$ = 5.4 Ω. When mounted onto the free end of the beam, the coil covers part of the beam by a length of 10.0 mm. The actual experiment setup is shown in Fig. 5. Two laser displacement sensors were used to capture the output response of the vibrating base and the harvester at point P as labelled in Fig. 5, which is located at approximately $x = L + L^{mass} + 5.0$ mm. These sensors are connected to a data acquisition (DAQ) card to transfer the acquired data to a computer. The coil was connected in series to a load resistor and wired into the DAQ device. The DAQ process was initiated using LabVIEW. In the experiment, the optimum load resistance of the harvester was not determined experimentally but was calculated using Eq. (25) for simplicity.

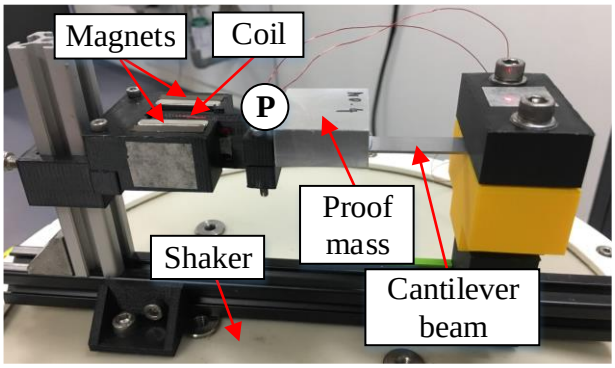


**Fig. 5.** Actual experimental setup to verify the mathematical model for the SDOF harvester.

The experiment was conducted for all four cantilever beams presented in Table 2. The dimensions and mechanical properties of each harvester are tabulated in Table 2, in where $\rho^{mass}$ refers to the density of the added proof mass. The mechanical properties of the materials were measured experimentally, whereas the thermal properties were obtained from the supplier's website [38]. The calculated first mode natural frequency, $\omega_1$, and optimum load resistance, $R_L^{opt}$, are also tabulated in Table 2.

**Table 2:** Mechanical and thermal properties and dimensions of four SDOF harvesters made of different materials.

| Material | Aluminium | Stainless Steel | Glass Fibre | PVC |
|---|---|---|---|---|
| $E$ (GPa) | 63.0 | 175.0 | 22.5 | 3.1 |
| $\sigma_f$ (MPa) | 86 | 183 | 54 | 12 |
| $\alpha$ ($\times 10^{-6}$) | 24.0 | 17.0 | 11.0 | 67.0 |
| $C_p$ ($\mathrm{Jkg^{-1}K^{-1}}$) | 900 | 500 | 1500 | 1000 |
| $k$ ($\mathrm{Wm^{-1}K^{-1}}$) | 222.0 | 13.8 | 0.42 | 0.15 |
| $\rho$ ($\mathrm{kgm^{-3}}$) | 2656 | 8125 | 1835 | 1360 |
| $L$ (mm) | 58.6 | 34.8 | 30.1 | 50.2 |
| $h$ (mm) | 1.20 | 1.00 | 1.63 | 2.38 |
| $w$ (mm) | 19.8 | 11.8 | 12.2 | 26.3 |
| $\rho^{mass}$ ($\mathrm{kgm^{-3}}$) | 7600 | 2700 | 2700 | 0 |
| $L^{mass}$ (mm) | 10.0 | 31.3 | 39.6 | 0 |
| $h^{mass}$(mm) | 10.0 | 14.1 | 13.2 | 0 |
| $w^{mass}$ (mm) | 25.0 | 38.0 | 38.0 | 0 |
| $\omega_1$ (Hz) | 23.0 | 26.6 | 19.9 | 29.4 |
| $R_L^{opt}$ (Ω) | 36.2 | 29.9 | 47.7 | 41.2 |

Each harvester was vibrated within a 4.0 Hz frequency range, ensuring that the first mode natural frequency lies within the specified frequency range. A base acceleration of $G$ = 0.1 $g$ (1 $g$ = 9.81 $\mathrm{ms^{-2}}$) was used in the experiments. Initially, the magnet component was removed and the experiments were conducted without the magnets to verify the damping stress equations presented in Table 1. Fig. 6 demonstrates the comparison between the experimental and theoretical absolute amplitude, $z_a$, of each individual harvester at point P (Fig. 5).

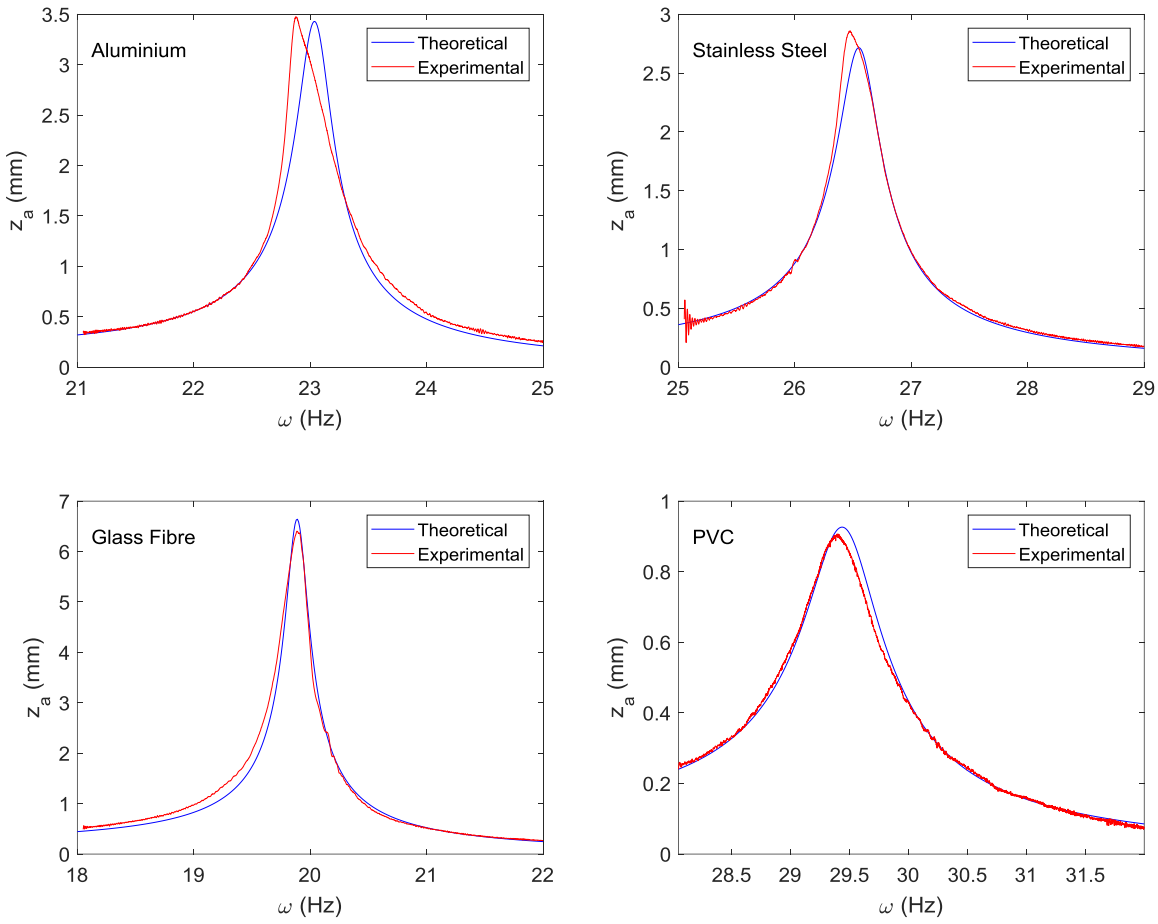


**Fig. 6.** Comparison between theoretical and experimental results for the absolute amplitude at position P for aluminium, stainless steel, glass fibre and PVC harvesters under zero electromagnetic damping condition.

Overall, the experimental results demonstrate a good agreement with the theoretical results with an average error of less than 2.9% and 4.7% in terms of $\omega_1$ and peak $z_a$ value respectively. This shows that the application of the damping stress equation implemented in this study is effective. A slight skewness can be observed in the response output for the aluminium and stainless steel harvester, which caused a larger discrepancy between their experimental and theoretical values for $\omega_1$. It is believed that this is caused by the non-linear stiffening effect due to high amplitude vibrations and many repeated tests, which are more prominent in metallic materials [39]. The magnets were then clamped onto the shaker and the response of the harvester at point P was re-taken. Additionally, the RMS voltage output of the harvester at the load resistance, $V_{rms}$, was also recorded as seen in Fig. 7. In the theoretical model, the $V_{rms}$ value was evaluated based on Eq. (1), where $x_c = L^{mass} + 27.0$ mm.

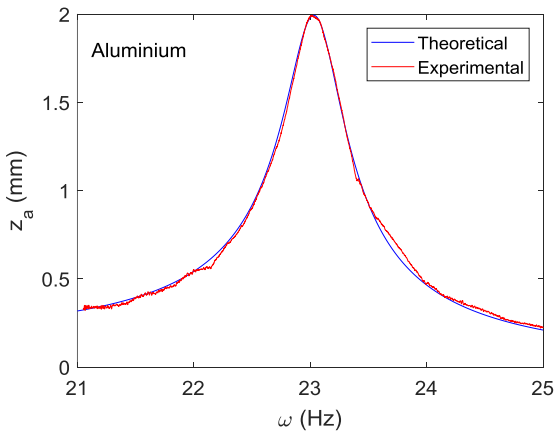
Aluminium
Theoretical
Experimental
$z_a$ (mm)
$\omega$ (Hz)

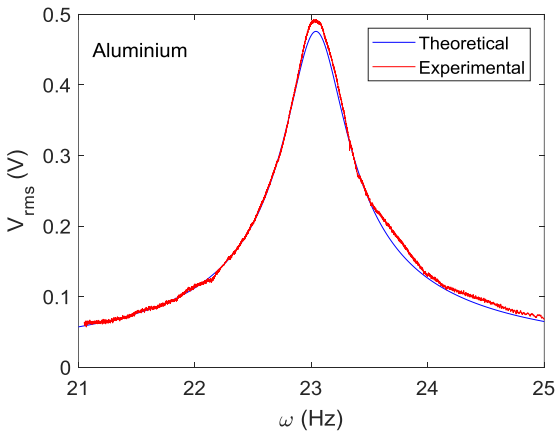
Aluminium
Theoretical
Experimental
$V_{rms}$ (V)
$\omega$ (Hz)

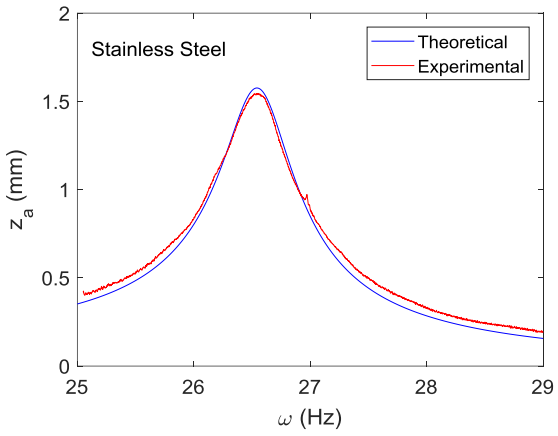
Stainless Steel
Theoretical
Experimental
$z_a$ (mm)
$\omega$ (Hz)

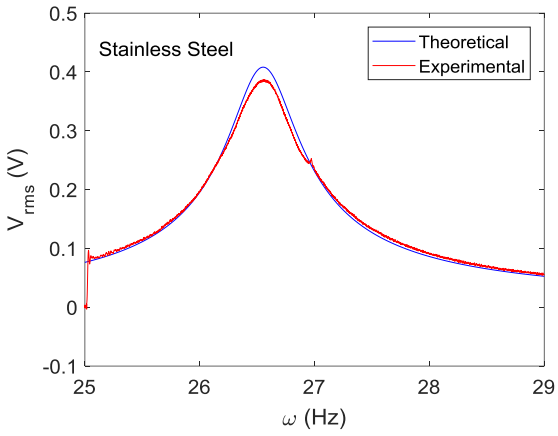
Stainless Steel
Theoretical
Experimental
$V_{rms}$ (V)
$\omega$ (Hz)

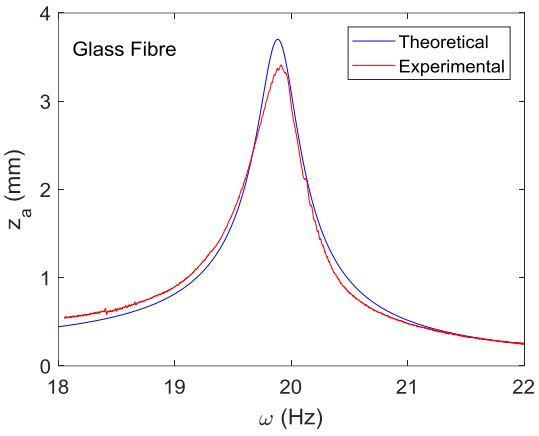
Glass Fibre
Theoretical
Experimental
$z_a$ (mm)
$\omega$ (Hz)

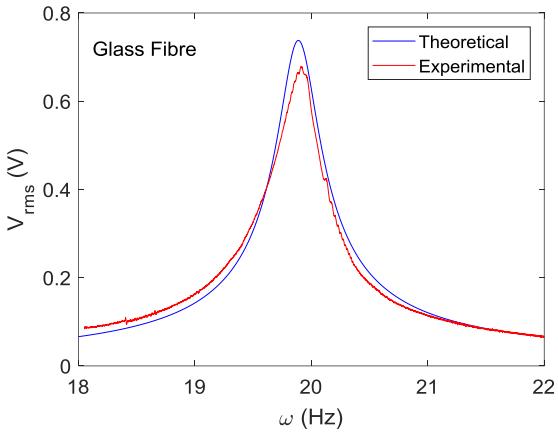
Glass Fibre
Theoretical
Experimental
$V_{rms}$ (V)
$\omega$ (Hz)

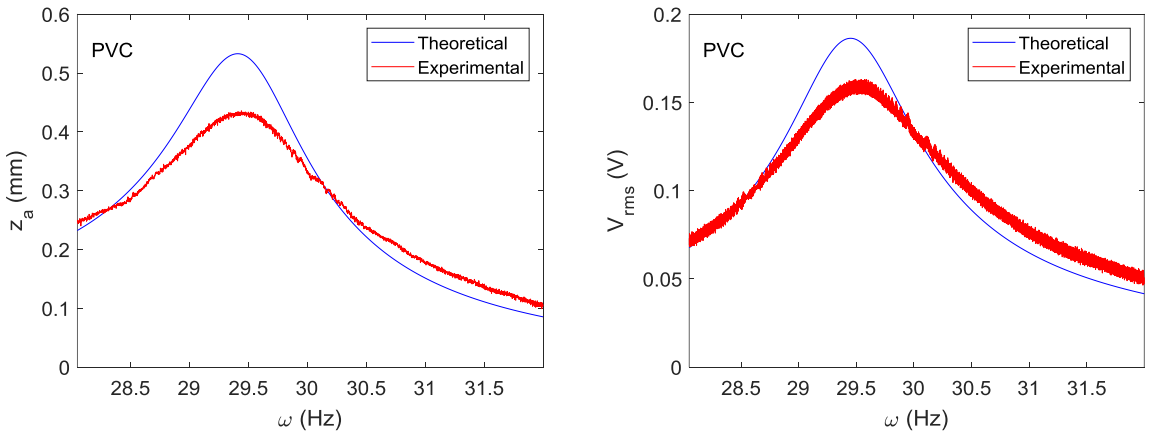


**Fig. 7.** Comparison between theoretical and experimental results for the absolute amplitude at position P and the corresponding voltage output for aluminium, stainless steel, glass fibre and PVC harvesters under the optimum load resistance condition.

A good agreement can be observed between experimental results and the theoretical model for the aluminium, glass fibre and stainless steel harvester, with an error of less than 8.8% in terms of both peak $z_a$ and peak $V_{rms}$ value. However, the PVC harvester displayed a significantly lower amplitude and voltage in the experiment as compared to its theoretical model. This suggests that the PVC harvester experienced a higher electromagnetic damping than what was predicted using Eq. (12). The reason for this is that in Eq. (2), a single averaged magnetic flux value was used to approximate the entire magnetic flux that is in contact with the coil. In reality, the magnetic flux of the permanent magnets is not constant and changes in the direction along the height of the magnets. Since the amplitude of the PVC beam is much smaller than the other materials, it suggests that the average flux value used in the theoretical model would hold for larger amplitude cases or in other words, materials with relatively small mechanical damping ratios such as aluminium, stainless steel and glass fibre. Consequently, because the PVC material recorded the lowest amplitude and voltage output among all other materials, it would be the least practical choice for vibration energy harvesting applications. Therefore, this material will be excluded from further analysis. Nevertheless, the damping stress equation developed for the PVC harvester is still valid based on the strong agreement observed in Fig. 6 during the absence of the electromagnetic interaction. The comparison between the experimental and theoretical maximum averaged power output for the aluminium, stainless steel and glass fibre harvesters are tabulated in Table 3.

**Table 3.** Comparison between experimental and theoretical power outputs for three different SDOF harvesters.

| Material | Aluminium | Stainless Steel | Glass Fibre |
|---|---|---|---|
| Experimental $P_{ave}$ (mW) | 6.5 | 5.0 | 9.8 |
| Theoretical $P_{ave}$ (mW) | 6.1 | 5.6 | 11.5 |

From Table 3, the glass fibre harvester has the largest error when compared with the theoretical results, raising up to 17.3% in difference. However, since the power is proportional to the velocity squared, this difference still lies within the margin of error discussed earlier. Overall, it can be concluded that the theoretical model and the damping evaluation methods presented in this paper are in good agreement with the experimental results, hence validating the governing equations.

## 6. Practical volume and load resistance considerations for a SDOF electromagnetic harvester

Usually, one would assume that the power output of a harvester is proportional to its volume. This generally means that a larger harvester would generate more power. Additionally, one would also consider the optimum load resistance condition to maximise the power output of the harvester.

However, these claims may not be true under certain conditions. To verify this, a structural optimisation was performed on a cantilever-based electromagnetic vibration energy harvester using aluminium, stainless steel and glass fibre cantilever beams based on the same harvester design as in Fig. 2. A steel cuboid proof mass was considered in the optimisation. The optimisation problem was solved using the constrained optimisation function in MATLAB, which applies the interior-point algorithm to solve linear and non-linear constrained problems. Table 4 below list down the objective function to maximise and the constraints applied in the optimisation. The criteria for Euler-Bernoulli beam from Eqs. (17) and (18) were also included in the constraints. As not all beam thickness, $h$, are readily available from suppliers, the optimisation was conducted under cases of constrained and non-constrained beam thickness. For the first case, the beam thickness was constrained to the values presented in Table 2. The same coil and magnets used in the verification were also applied in the optimisation problem.

**Table 4:** Objective function and constraints applied to the structural optimisation problem for the SDOF harvester.

| Objective function |
|---|
| Maximise: |
| $P_{ave} = f(L, h, w, L^{mass}, w^{mass}, h^{mass})$ |
| **Constraints** |
| 8.0 mm $< w \leq$ 27.0 mm |
| $L \geq 10h$ |
| $\rho^{mass}$ = 7800 kgm$^{-3}$ |
| $h, L^{mass}, w^{mass}, h^{mass} > 0$ |
| $w^2 M \leq EIh$ |
| $G$ = 0.1 $g$ |
| $\omega_1$ = 25.0 Hz |
| $\lvert\sigma_{max}\rvert \leq 0.8\sigma_f$ |
| $(L + L^{mass} + L^{mc}) w_p h_p \leq V_p$ |

The beam width was constrained between 8.0 mm and 27.0 mm based on the selected coil component. The first mode natural frequency of the harvester was chosen to be fixed at 25.0 Hz. The last row in Table 4 defines a cuboid representation of the practical volume of the harvester, $V_p$, which takes into account the maximum swept volume of the harvester during operation. The said volume is inclusive of the magnet component, where $L^{mc}$ corresponds to a constant length occupied by the coil and the magnets, measuring 65.0 mm. The variables $w_p$ and $h_p$ are the width and the swept height of the harvester measured at first mode resonance. These variables are determined based on the width and height of the beam, coil, magnets and proof mass as well as the harvester's amplitude. Finally, the maximum stress of the harvester during operation was limited to 80.0% of its fatigue limit stress that were tabulated in Table 2.

The optimisation process was initiated at 50 different initial conditions to minimise the risk of finding a local maximum. The optimisation problem in Table 3 was applied to the three mentioned cantilever beam materials for a constrained practical volume of 150 cm$^3$ $\leq V_p \leq$ 500 cm$^3$ in intervals of 50 cm$^3$. Normally, optimisation is usually performed under the condition of optimum load resistance ($R_L = R_L^{opt}$) as one would want to maximise the power output of the harvester, which occurs at the optimum load resistance. This means that the case of where the harvester is operating at $R_L \neq R_L^{opt}$ was not considered in the optimisation. However, there may exist situations where due to the applied constraints, the maximum power achievable by the harvester is not located at the optimum load resistance. To analyse this, the load resistance was defined as a parameter of the objective function in Table 4, $P_{ave} = f(L, h, w, L^{mass}, w^{mass}, h^{mass}, R_L)$, and constraint to values more than zero, $R_L > 0$. The optimisation problem was then repeated for the same two cases of fixed and non-

constrained beam thickness. Fig. 8 describes the variation of the optimum average power output, $P_{ave}$ and RMS voltage output, $V_{rms}$ against $V_p$ for the three beam materials under the conditions of $R_L^{opt}$ and $R_L$ as a parameter, $R_L^p$. It is worth to mention that for each different practical volume constraints, the optimum solution resulted in a geometry that converged to the limit of this constraint, meaning that if the volume was constrained to $V_p$ = 500 cm$^3$, then the optimised solution would maximise the geometry of the harvester to achieve 500 cm$^3$ for maximum power output.

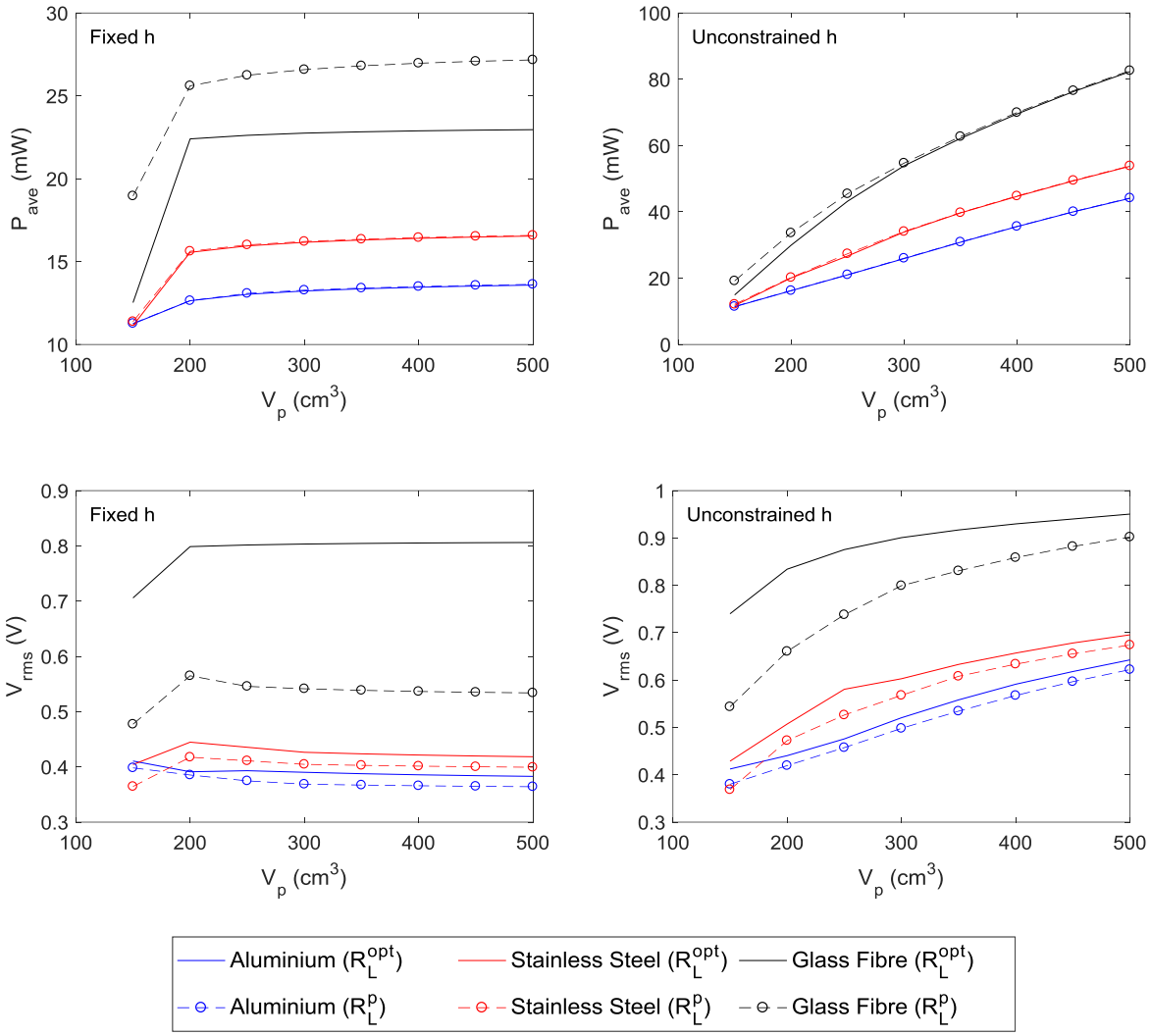


**Fig. 8.** Optimised SDOF harvester power output (top row) and voltage output (bottom row) against the practical volume constraint for fixed and unconstrained beam thickness condition.

Results in Fig. 8 shows that for the set constraints, the glass fibre cantilever beam would generate the highest power output for both cases of fixed and unconstraint beam thickness. Under the case of a fixed beam thickness, the power and voltage outputs of the harvesters are seen to converge and remain approximately the same despite the increase in the practical volume. In terms of design, this analysis demonstrates the irrelevance of considering a larger volume space if the thickness of the beam and the electromagnetic components are constrained since a similar power output can be obtained at a much smaller volume. However, if the beam thickness was not constrained, significant increase in the power and voltage output can be observed with increasing volume.

For the stainless steel and aluminium beam, the condition of $R_L^{opt}$ and $R_L^p$ lead to a very similar result in terms of power output for both cases of constrained and unconstrained thickness. However,

the voltage output under the condition of $R_L^p$ can be up to 19.0% lower than the voltage output under the $R_L^{opt}$ condition. This is because the magnitude of $R_L^p$ was recorded to be lower than $R_L^{opt}$ for all the performed optimisations. On the other hand, under a fixed beam thickness, the glass fibre harvester displayed a significant (17.8%) increase in power output under the condition of $R_L^p$ as compared to $R_L^{opt}$, although a lower voltage output was also recorded. In the case of unconstrained beam thickness, the glass fibre harvester demonstrated a similar power output under the $R_L^{opt}$ and $R_L^p$ conditions at higher practical volumes. However, the voltage output under the condition of $R_L^p$ was much lower as compared to the $R_L^{opt}$ condition. The reason that the glass fibre harvester displayed a better power output in the fixed beam thickness case under the condition of $R_L^p$ is because glass fibre has a low fatigue stress limit and also a low damping capacity. This makes it harder for the glass fibre harvester to achieve the set stress constraint in Table 4 since a low damping generally leads to a higher amplitude and stress, therefore limiting the range of possible variations in the optimisation especially since the beam thickness was fixed. When coupled with the $R_L^{opt}$ condition, the optimisation becomes more limited as the electromagnetic damping of the harvester under the $R_L^{opt}$ condition is always lower than the mechanical damping, making it harder to achieve a lower stress. Stainless steel and aluminium have a higher fatigue limit stress, allowing more room for optimisation. Additionally, the final stress value corresponding to the optimised parameters of the stainless steel and aluminium harvesters did not reach the stress limit set in Table 4, unlike the glass fibre harvester. Overall, this analysis suggest that to maximise the performance of a SDOF electromagnetic harvester, the $R_L^{opt}$ condition should be considered when optimising for materials with a high fatigue limit stress whereas the $R_L^p$ condition should be used for materials that has a low fatigue limit stress and damping.

## 7. Power limit of a SDOF electromagnetic harvester

In an earlier study, William and Yates [40] showed that under the uncoupled conditions, there exists a power limit for a specific vibration energy harvester. This means that for a specific base input and natural frequency, the power output of the harvester cannot exceed a certain value regardless of how high the electromagnetic coupling factor is. The power limit for a cantilever-based electromagnetic vibration energy harvester can be derived by considering the condition of $R_L^{opt}$ and substituting Eq. (25) into Eq. (24).

$$P_{ave} = \left\{\frac{1}{2\sqrt{2d_c}} m_e G F_1[\varphi_1(L) + x_c\varphi_1{}'(L)]\right\}^2 \frac{K^2/R_c}{K^2/R_c + d_c} \tag{26}$$

Here, $K^2/R_c$ is designated as the electromagnetic coupling coefficient of the harvester. It is easy to notice that as $K^2/R_c \to \infty$,

$$\frac{K^2/R_c}{K^2/R_c + d_c} \to 1 \tag{27}$$

Eq. (27) holds true even when $N$, $B$, $l$ or $f$ were to be increased indefinitely. This shows that the power limit, $P_{lim}$, of the harvester when $K^2/R_c \to \infty$ is

$$P_{lim} = \frac{1}{8d_c} {m_e}^2 G^2 {F_1}^2 [\varphi_1(L) + x_c\varphi_1{}'(L)]^2 \tag{28}$$

Eq. (28) is observed to be independent of its electromagnetic parameters. With a bit of effort, it can be shown that Eq. (28) meets the criteria of optimum load resistance when $K^2/d_c \gg R_c$, which is $\zeta_e = \zeta_m$. Eq. (28) can be optimized to show the maximum power limit of the harvester. In addition, Eq. (28) also highlights the importance of maximizing the electromagnetic coupling coefficient to obtain a higher power output when considering the optimum load resistance.

Note that the power limit of the harvester is only defined under the optimum load resistance condition since this condition corresponds to the maximum power output of the specific harvester. Fig. 9 below describes the optimized practical $P_{lim}$ output of each beam material in Table 3 for different $V_p$ values under a constant base acceleration of 0.1 $g$ and a fixed fundamental natural frequency of 25.0 Hz. The same constraints as in Table 4 were applied and the same steel material was used for the proof mass. It was assumed that $K^2/R_c$ was increased by increasing $B$, therefore retaining the same inertial terms.

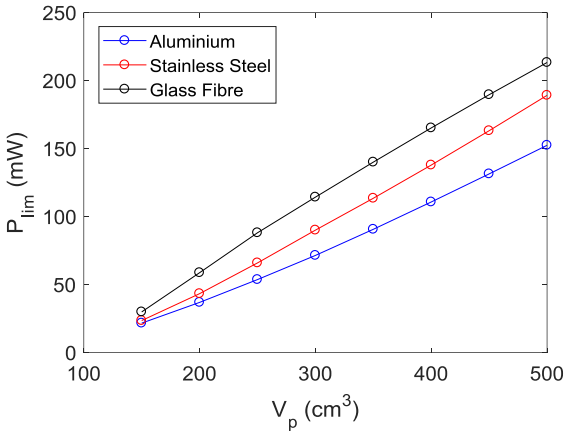


**Fig. 9.** Optimised SDOF harvester power limit against practical volume constraint for aluminium, stainless steel and glass fibre harvesters.

Overall, the results in Fig. 9 show an increase in $P_{lim}$ when the practical volume increases, which has been commonly understood. Is can be observed that for all practical volumes, the glass fibre harvester demonstrates the highest power limit. The aluminium harvester beam displayed the lowest overall power limit for all practical volumes due to its higher damping. Generally, knowing the power limit of a harvester one can give an idea on the capacity of the harvester. For example, using the same coil, magnets and proof mass material, if one wishes to generate an average power output of 45.0 mW for a vibrating base input of 0.1 $g$ at 25 Hz within a constrained space of 200.0 cm$^3$, the only possible material that can achieve this would be glass fibre. On the other hand, it would be impossible to achieve an average power output of 70.0 mW within the same volume space for any of the beam materials presented in Fig. 9.

The power limit presented by Eq. (28) and Fig. 9 is under the ideal condition, where $K^2/R_c \to \infty$, which may be difficult to achieve in practical applications. Therefore, a more practical approach would be to investigate the fraction of $P_{lim}$ that is practically achievable. Based of Eq. (27), to get as close as to Eq. (28), $K^2/R_c$ must be much greater than the mechanical damping constant of the harvester, $d_c$. The smaller $d_c$ is, the lower the coupling coefficient required to achieve a power output that is closer to $P_{lim}$. However, at higher practical volumes, the optimized dimension of the harvester tends to achieve a higher damping coefficient due to the increase in the effective mass. Fig. 10 (left) describes the variation in $d_c$ against $V_p$ for the results presented in Fig. 10. The current coil and magnet arrangement used in the experiment has an electromagnetic coupling coefficient of $K^2/R_c$ = 0.65 kgs$^{-1}$. If the horizontal distance between the magnets were to reduce until the gap between the magnets and the coil was 0.1 mm, the average magnetic flux density of the magnets would increase to 0.46 T, making it possible to achieve a coupling coefficient value of approximately $K^2/R_c$ = 2.0 kgs$^{-1}$. Generally, a coupling coefficient larger than 1.0 kgs$^{-1}$ is considered to be high. Assuming a coupling value of $K^2/R_c$ = 2.0 kgs$^{-1}$ and that the optimised parameters from Fig. 9 are unchanged, Fig. 10 (right) describes the achievable $P_{ave}$ as a fraction of $P_{lim}$. This assumption however is an underestimation since the optimized parameters change for different coupling coefficient values and would result in a slightly higher power output than the results presented in Fig. 10.

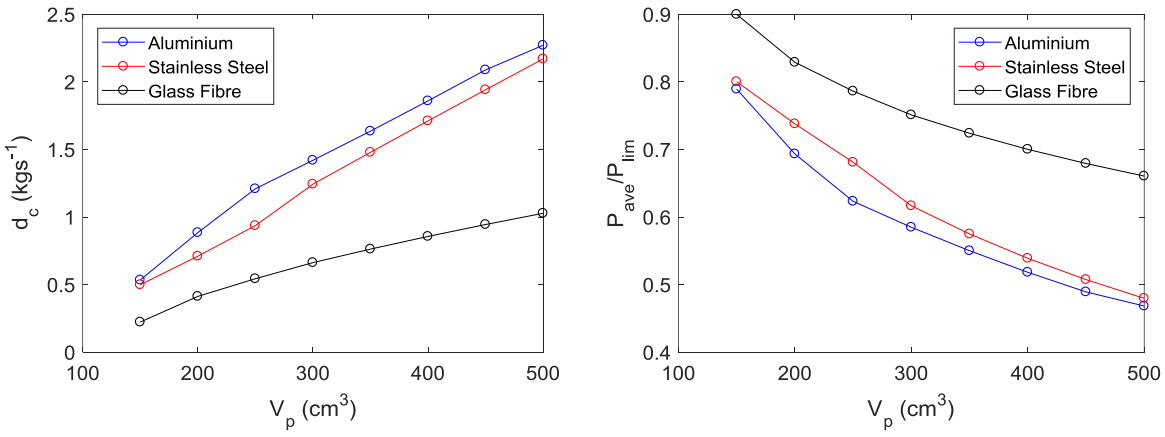


**Fig. 10.** Variation in mechanical damping constant (left) and ratio of power output to power limit (right) against the practical volume constraint for aluminium, stainless steel and glass fibre harvesters.

Fig. 10 shows that at lower practical volumes, it is possible to achieve a high portion of $P_{lim}$ when considering a high electromagnetic coupling value In other words, approximately 80.0% of $P_{lim}$ is considered achievable under these volumes. However, the percentage of achievable $P_{lim}$ drops as the practical volume increases due to the increase in the mechanical damping constant, although the actual value of $P_{ave}$ increases with increasing $V_p$ as was seen in Fig. 8. In other words, this means that the capability of the harvester to reach its maximum power output decreases with damping or volume. William and Yates [40] and Stephen [41] have both modelled an identical equation for SDOF vibration energy harvesters which one describes as the harvester's maximum power output whereas the latter defined it as the power flow into the harvester. Based on this argument, if $P_{lim}$ was assumed to be equal to the power supplied to the harvester, $P_{ave}/P_{lim}$ would indicate the efficiency of the harvester, which decreases with increasing volume. A higher efficiency ratio may be possible if a larger electromagnetic coupling value was obtained or if the damping constant of the harvester was reduced. Nevertheless, despite the drop in efficiency with increasing $V_p$, the actual magnitude of $P_{ave}$ still increases with increasing $V_p$.

Overall, the study here shows that considering a high $K^2/R_c$ value, the ratio of $P_{ave}/P_{lim}$ decreases with increasing practical volume when the structural aspect of the harvester was optimised due to the increase in $d_c$. This means that it is important to first select a material that has a low damping capacity for the harvester to achieve a higher $P_{ave}/P_{lim}$ value. However, if the material of the harvester could not be changed due to the requirements of a particular application, the mechanical damping parameter would then be generally difficult to control as it has a complex relation with many structural parameters. One may suggest reducing the effective mass on the harvester as this would reduce the value of $d_c$. However, in doing so it would also cause the power limit of the harvester to decrease according to Eq. (28), which would then result in a decrease of the average power output. In fact, in this case, it would be more desirable to increase the effective mass to obtain a larger power output and to also maximise the value of $K^2/R_c$ by optimising the electromagnetic aspect in order to increase the ratio of $P_{ave}/P_{lim}$.

## 8. Proof mass considerations for a SDOF electromagnetic harvester.

The results presented so far were under the assumption of a cuboid shaped proof mass and a constant inertial term for the coil component that is fixed at the free end of the cantilever beam. Generally, the inertial term of an object placed on a cantilever beam plays an important role on the power output of the harvester. The inertial term of an object is dependent on both its shape and its mass. Hence, it would be interesting to know as to how the mass, inertial term and centre of gravity of a proof mass placed onto the free end of a cantilever beam effects the performance of a SDOF

cantilever-based electromagnetic vibration energy harvester. To analyse this, an optimisation was performed for the aluminium cantilever beam by making the mass, inertial terms and centre of gravity of an arbitrary mass as a function of the average power output. For simplicity, it was assumed that the mass is symmetrical along its width and it is attached rigidly to the free end of the beam as seen in Fig. 11.

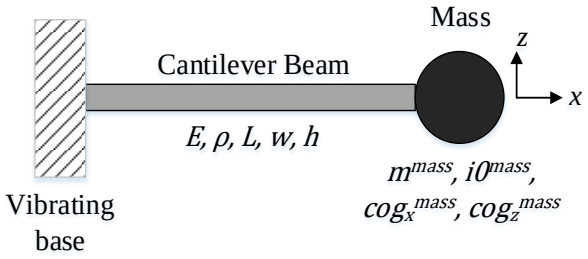


**Fig. 11.** Considerations of four different parameters to analyse the effect of an arbitrary proof mass geometry and mass on the power output of an electromagnetic vibration energy harvester

Here, $m^{mass}$, $i0^{mass}$, ${cog_x}^{mass}$, ${cog_z}^{mass}$ defines the mass, moment of inertia at the centre of gravity and the centre of gravity in the $x$ and $z$ direction of the arbitrary mass. Note that the circular shape of the proof mass in Fig. 11 is only a figurative representation and does not reflect the true shape of the mass. Furthermore, $i0^{mass}$ only defines the shape contribution of the inertial term. Table 5 describes the objective function and constraints applied in the optimisation problem. Both conditions of optimum load resistance and load resistance as a parameter were considered in this analysis.

**Table 5.** Objective function and constraints applied to the arbitrary mass optimisation problem for the SDOF harvester.

| Objective function |
|---|
| Maximise: |
| $P_{ave} = f(L, h, w, m^{mass}, i0^{mass}, {cog_x}^{mass}, {cog_z}^{mass})$ |
| **Constraints** |
| $L \geq 10h$ |
| $h, w > 0$ |
| $0 \leq m^{mass}, i0^{mass}, {cog_x}^{mass}, {cog_z}^{mass} \leq u_L$ |
| $w^2 M \leq EIh$ |
| $G$ = 0.1 $g$ |
| $\omega_1$ = 25.0 Hz |
| $\lvert\sigma_{max}\rvert \leq 0.8\sigma_f$ |
| $(L + 2{cog_x}^{mass})wh_p \leq$ 200.0 cm$^3$ |

The practical volume specified in Table 5 is an approximation as the actual shape of the mass is actually unknown. However, the actual volume is not important as the focus of this analysis is to observe the convergence of variables $m^{mass}$, $i0^{mass}$, ${cog_x}^{mass}$ and ${cog_z}^{mass}$ in the optimization problem, where $u_L$ defines an arbitrary upper limit for the specified variables. Fig. 12 illustrates the variation in variables $m^{mass}$, $i0^{mass}$, ${cog_x}^{mass}$ and ${cog_z}^{mass}$ normalized by the upper limit, $u_L$, against the number of iterations in the optimisation problem for cases of $R_L^{opt}$ and $R_L^p$.

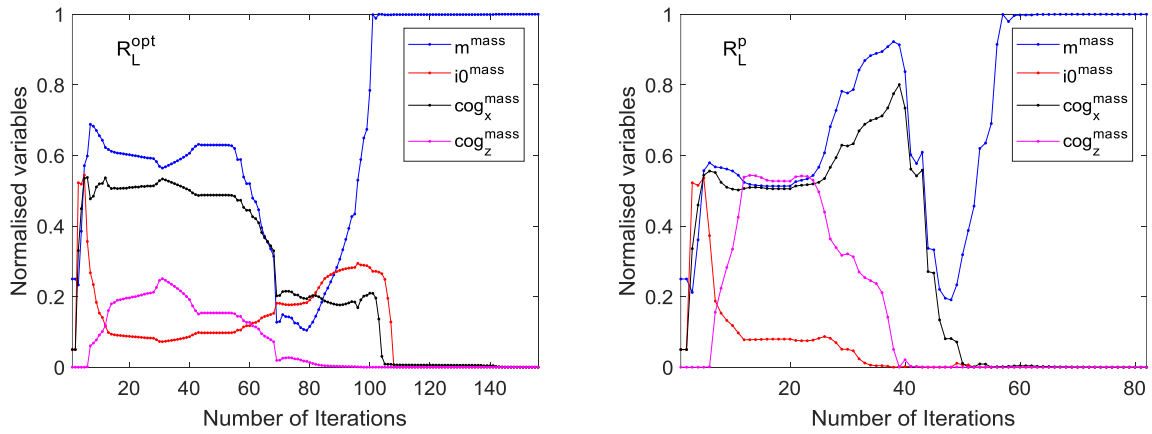


**Fig. 12.** Variation in the arbitrary mass's normalised mass and inertial terms with number of iterations for $R_L^{opt}$ (left) and $R_L^p$ (right) condition.

Fig. 12 shows that $m^{mass}$ converges to the set upper limit, whereas $i0^{mass}$, ${cog_x}^{mass}$ and ${cog_z}^{mass}$ converges to zero for the harvester to achieve its optimum average power output. The same trend was observed in both cases of $R_L^{opt}$ and $R_L^p$. The analysis suggests that the best type of mass to attach at the free end of the electromagnetic vibration energy harvester to maximise its power is actually in a form of a point mass. It is practically unrealistic to make the coil or magnets attached on the harvester to resemble a point mass and usually, the topology of these components are pre-determined and difficult to adjust. However, it is possible to change the properties of the additional proof mass added for the purpose of tuning the natural frequency of the harvester. Based on Fig. 8, one can deduce that the best method to increase the mass and reduce the inertial term of a proof mass is by using a material of high density such as tungsten. This way, a larger mass can be achieved for a smaller volume and hence a smaller inertial term. Moreover, to reduce the inertial terms also means that the proof mass must be placed as close as possible to $x = L$ on the beam. Ideally, the centre of gravity of the mass should lie exactly on this position. However, this may be difficult depending on designs since a large mass may interfere with the vibration of the coil between the magnets. Considering the current coil and magnet design as in Fig. 1, a good location to place the proof mass would be similar to the layout shown in Fig. 4.

To verify this argument, the optimisation problem conducted in Table 4 was repeated for the aluminium harvester using different proof mass densities ranging between $0 \leq \rho^{mass} \leq 25000$ kgm$^{-3}$, under a constrained volume of $V_p$ = 200 cm$^3$ and using the same coil and magnets as in the experiment. The beam thickness of the aluminium harvester was fixed the value given in Table 2 for a more practical comparison. In this analysis, the condition of optimum load resistance was implemented. Fig. 13 below illustrates the results of the analysis. The red marking indicates the average power output and RMS voltage output of the aluminium beam when using a steel proof mass as recorded in Fig. 8.

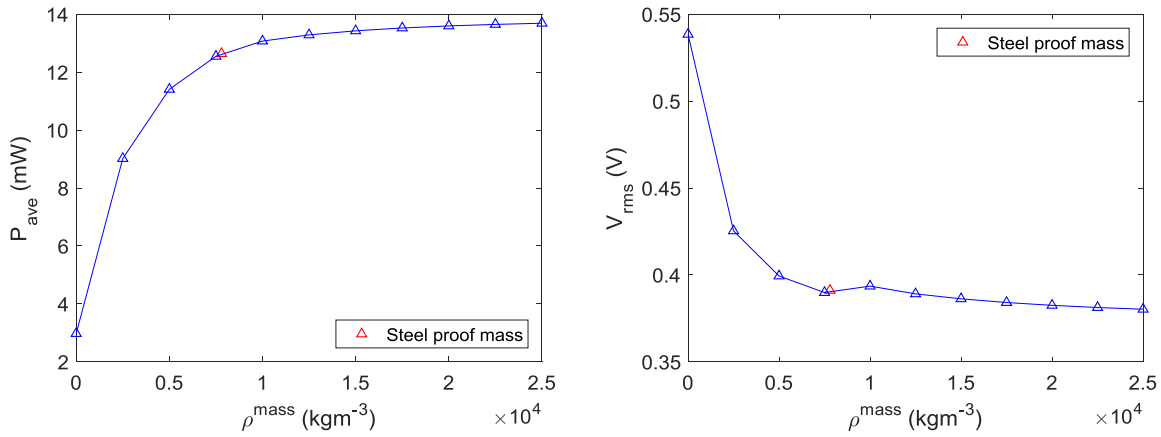


**Fig. 13.** Variation in power output (left) and voltage output (right) with proof mass density for an aluminium harvester with a steel proof mass.

Fig. 13 demonstrates an increase in average power output when the density of the proof mass increases. On the other hand, the generated voltage is observed to decrease when using a higher density proof mass. It can be observed that the increase in power output is much more significant at lower proof mass density as compared to higher ones. The same observation can be made for the decrease in voltage output. The increase in power between a tungsten ($\rho^{mass}$ = 19300 kgm$^{-3}$) proof mass when compared to an aluminium ($\rho^{mass}$ = 2700 kgm$^{-3}$) proof mass is approximately 50.8%, with a 10.1% drop in voltage whereas if the tungsten proof mass was compared to a steel ($\rho^{mass}$ = 7800 kgm$^{-3}$) proof mass, the increase in power is only 7.6%, with a 2.2% drop in voltage. Nevertheless, this highlights the importance of using a high-density proof mass to maximise the power output of an electromagnetic vibration energy harvesters.

## 9. Conclusion

This study examines several important considerations that must be made when optimising the structural aspects of a SDOF electromagnetic vibration energy harvester. The harvester considered adopts the typical cantilever beam design and is excited at its clamped end. Firstly, the mathematical models for the power output and the damping ratio of the SDOF harvester were derived from the Euler-Bernoulli beam theory and the critically damped stress method. The models were experimentally verified for four different cantilever beam materials. While the experimental results of three materials displayed an excellent agreement with the theoretical derivations, the electromagnetic damping model predicted a lower damping for the PVC beam when compared to the experimental value. Hence, this material was excluded in further analysis. A structural optimisation was then performed on the remaining three materials by varying the dimensions of the cantilever beam and the proof mass, while maintaining the same electromagnetic components. It was concluded that if the thickness of the cantilever beam was fixed, the increase in the power output of the harvester with volume becomes insignificant at larger volumes. This means that for this case, it is more practical to consider a smaller volume. In addition, it was shown that for materials with a low damping capacity and a low fatigue limit stress, it is better to consider the $R_L^p$ condition in the optimisation instead of the $R_L^{opt}$ condition to achieve a higher power output. Further analysis demonstrated the existence of a power limit that defines the maximum achievable power of an electromagnetic harvester when the electromagnetic coupling coefficient approaches infinity. It was observed that approximately 80.0% of the power limit can be achieved for low damping harvesters when considering a high electromagnetic coupling coefficient value and a small volume constraint. While this ratio was seen to decreases with increasing practical volume, the actual power output increases at larger volumes. The analysis has also shown that the ideal proof mass to maximise the power output of a SDOF harvester is a point mass. While this is not practical, it suggests the importance of considering a high density proof mass that is centred

as close as possible to the free end of the cantilever beam. Although the analysis conducted in this study are based on the cantilever beam design, the results presented would be applicable for other SDOF electromagnetic vibration energy harvester designs.

## References


[1] J. Chen, Z.L. Wong, Reviving Vibration Energy Harvesting and Self-Powered Sensing by a Triboelectric Nanogenerator, Joule 1 (2017) 480–521.

[2] Y. Naito, K. Uenishi, Electrostatic MEMS Vibration Energy Harvesters inside of Tire Treads, Sensors 19 (2019) 890.

[3] S. Fang, X. Fu, W.H. Liao, Modeling and experimental validation on the interference of mechanical plucking energy harvesting, Mech. Syst. Signal Process. 134 (2019) 106317.

[4] X. Tang, L. Zuo, Large-scale vibration energy harvesting, J. Intell. Mater. Syst. Struct. 24(11) (2013) 1405–1430.

[5] J.J. Wang, G.P. Penamalli, L. Zuo, Electromagnetic Energy Harvesting from Train Induced Railway Track Vibrations, in: 8th IEEE/ASME International Conference Mechatronic Embedded System Application, Institute of Electrical and Electronics Engineers, 2012, pp. 29–34.

[6] I.L. Cassidy, J.T. Scruggs, S. Behrens, H.P. Gavin, Design and experimental characterization of an electromagnetic transducer for large-scale vibratory energy harvesting applications, J. Intell. Mater. Syst. Struct. 22(17) (2011) 2009–2024.

[7] Z. Liu, X. Wang, R. Zhang, L. Wang, A Dimensionless Parameter Analysis of a Cylindrical Tube Electromagnetic Vibration Energy Harvester and Its Oscillator Nonlinearity Effect, Energies 11 (2018) 1653.

[8] E. Dechant, F. Fedulov, D.V. Chashin, L.Y. Fetisov, Y.K. Fetisov, M. Shamonin, Low-frequency, broadband vibration energy harvester using coupled oscillators and frequency up-conversion by mechanical stoppers, Smart Mater Struct. 26(6) (2017) 065021.

[9] B.L. Ooi, J.M. Gilbert, Design of wideband vibration-based electromagnetic generator by means of dual-resonator, Sens. Actuat. A: Physical 213 (2014) 9–18.

[10] C.K. Thein, J.S. Liu, Numerical modeling of shape and topology optimisation of a piezoelectric cantilever beam in an energy‐harvesting sensor, Eng. Comp. 33 (2017) 137–148.

[11] W.C. Tai, L. Zuo, On optimization of energy harvesting from base-excited vibration, J. Sound Vib. 411 (2017) 47–59.

[12] X. Tang, L. Zuo, Enhanced vibration energy harvesting using dual-mass systems, J. Sound Vib. 330(21) (2011) 5199–5209.

[13] M. Hendijanizadeh, S.M. Sharkh, S.J. Elliott, M. Moshrefi-Torbati, Output power and efficiency of electromagnetic energy harvesting systems with constrained range of motion, Smart Mater. Struct. 22 (2013) 125009.

[14] X. Liu, J. Qiu J, H. Chen, X. Xu, Y. Wen, P. Li, Design and Optimization of an Electromagnetic Vibration Energy Harvester Using Dual Halbach Arrays, IEEE Trans. Magnetics 51(11) (2011) 1–4.

[15] R. Zhang, X. Wang, H. Shu, S. John, The effects of the electro-mechanical coupling and Halbach magnet pattern on energy harvesting performance of a two degree of freedom electromagnetic vibration energy harvester, J. Vehicle Noise Vib. 14(2) (2018) 124–146.

[16] Y. Lei, Z. Wen, L. Chen, Simulation and testing of a micro electromagnetic energy harvester for self-powered system, AIP Adv. 4 (2014) 031303.

[17] D. Spreeman, Y. Manoli, Electromagnetic Vibration Energy Harvesting Devices, Germany: Springer 2012.

[18] S.P. Beeby, R.N Torah, M.J. Tudor, P. Glynne-Jones, T. O'Donnell, C.R. Saha, S. Roy, A micro electromagnetic generator for vibration energy harvesting, J. Micromech. Microeng. 17 (2007) 1257–1265.

[19] X. Tang, T. Lei, L. Zuo, Design and Optimization of a Tubular Linear Electromagnetic Vibration Energy Harvester, IEEE/ASME Trans. Mechatronics 19(2) (2014) 615–622.

[20] T. Kapanen, Optimizing electromagnetic vibration energy harvester for wireless sensor node, Masters Thesis, 2016.

[21] M.C. Chiu, Y.C. Chang, L.J. Yeh, C.H. Chung, Optimization of a two-mass vibration based electromagnetic energy harvester using simulated annealing method, J. Low Freq. Noise Vib. Active Control 37(1) (2018) 90–106.

[22] E.F. Joubaneh, O.R. Barry, On the Improvement of Vibration Mitigation and Energy Harvesting Using Electromagnetic Vibration Absorber-Inerter: Exact H2 Optimization, J. Vib. Acoust. 141(6) (2019) 061007.

[23] Z. Liu, X. Wang, S. Ding, R. Zhang, L. McNabb, A new concept of speed amplified nonlinear electromagnetic vibration energy harvester through fixed pulley wheel mechanisms and magnetic springs, Mech. Syst. Signal Process 126 (2019) 305–325.
[24] F. Cottone, R. Frizzell, S. Goyal, G. Kelly, J. Punch, Enhanced vibrational energy harvester based on velocity amplification, J. Intel Mater. Syst. Struct. 25(4) (2014) 443–441.
[25] J. Klein, L. Zuo, A velocity-amplified electromagnetic energy harvester for small amplitude vibration, Smart Mater. Sturct. 26(9) (2017) 095057.
[26] M.A. Halim, J.Y. Park, A frequency up-converted electromagnetic energy harvester using human hand-shaking, J. Phys: Conf. Ser. 476 (2013) 012119.
[27] A. Erturk, D.J. Inman, On mechanical modelling of cantilevered piezoelectric vibration energy harvesters, J. Intel. Mater. Syst. Struct. 19 (2007) 1311–1325.
[28] M. Kim, M. Hoegen, J. Dugundji, B.L. Wardle, Modeling and experimental verification of proof mass effects on vibration energy harvester performance, Smart Mater. Struct. 19 (2010) 045023.
[29] F.M. Foong, C.K. Thein, B.L. Ooi, D. Yurchenko, On mechanical damping of cantilever beam-based electromagnetic resonators, Mech. Syst. Signal Process. 119 (2019) 120–137.
[30] C. Zener, W. Otis, R. Nuckolls, Internal friction in solids III: Experimental demonstration of thermoelastic internal friction, Phys. Rev. 53 (1938) 100–101.
[31] R. Lifshitz, M. L. Roukes, Thermoelastic Damping in Micro- and Nano-Mechanical Systems, Phys. Rev. B. 61(8) (2000) 5600–5609.
[32] A. Labuschagne A, N.F.J. van Rensburg, A.J. van der Merwe, Comparison of linear beam theories, Math. Comp. Model 49 (2009) 20–30.
[33] M.E. Zamiralova, G. Lodewijks, Review of the troughability test ISO 703 for quantifying a uniform transverse bending stiffness for conveyor belts, Arch. Civil. Mech. Eng. 17 (2017) 249–270.
[34] C.K. Thein, F.M. Foong, Y.C. Shu, Damping ratio and power output prediction of an electromagnetic energy harvester designed through finite element analysis, Sens. Actuators A: Phys. 286 (2019) 220–231.
[35] B.J. Lazan, Damping of materials and members in structural mechanics, Pergamon Press, London, 1968.
[36] J.M. Lee, J.S. Moon, H. Lee, B.H. Choi, Investigation of fatigue and mechanical properties of the pipe grade poly(vinyl chloride) using recycled scraps, eXPRESS Polymer Lett. 9(4) (2015) 362–371.
[37] C.R. Saha, T. O'Donnell, H. Loder, S. Beeby, J. Tudor, Optimization of an Electromagnetic Energy Harvesting Device, IEEE Trans. Magnet. 42(10) (2006) 3509–3511.
[38] Material specifications. Retrieved November 7, 2019, from https://my.rs-online.com/.
[39] E. Habtour, D. Cole, J. Riddick, V. Weiss, M.E. Robeson, R. Sridharan, A. Dasgupta, Detection of fatigue damage precursor using a nonlinear vibration approach, Struct. Control Health Monit. 23(12) (2016) 1442–1463.
[40] C.B. Williams, R.B. Yates, Analysis of a micro-electric generator for microsystems, Sens. Actuat. A. 52 (1996) 8–11.
[41] N.G. Stephen, On energy harvesting from ambient vibration, J. Sound Vib. 293 (2006) 409–425.